Pattern of Auxin and Cytokinin Responses for Shoot Meristem Induction Results from the Regulation of Cytokinin Biosynthesis by AUXIN RESPONSE FACTOR3[1][W][OA]

Zhi Juan Cheng, Liang Wang, Wei Sun, Yan Zhang, Chao Zhou, Ying Hua Su, Wei Li, Tian Tian Sun, Xiang Yu Zhao, Xing Guo Li, Youfa Cheng[2], Yunde Zhao, Qi Xie, and Xian Sheng Zhang*

State Key Laboratory of Crop Biology, Shandong Key Laboratory of Crop Biology, College of Life Sciences, Shandong Agricultural University, Taian, Shandong 271018, China (Z.J.C., L.W., W.S., Y.Zhang, C.Z., Y.H.S., W.L., T.T.S., X.Y.Z., X.G.L., X.S.Z.); Section of Cell and Developmental Biology, University of California San Diego, La Jolla, California 92093–0116 (Y.C., Y.Zhao); and State Key Laboratory of Plant Genomics and National Plant Gene Research Center, Institute of Genetics and Developmental Biology, Chinese Academy of Sciences, Beijing 100101, China (Z.J.C., Q.X.)

De novo organ regeneration is an excellent biological system for the study of fundamental questions regarding stem cell initiation, cell fate determination, and hormone signaling. Despite the general belief that auxin and cytokinin responses interact to regulate de novo organ regeneration, the molecular mechanisms underlying such a cross talk are little understood. Here, we show that spatiotemporal biosynthesis and polar transport resulted in local auxin distribution in Arabidopsis (*Arabidopsis thaliana*), which in turn determined the cytokinin response during de novo shoot regeneration. Genetic and pharmacological interference of auxin distribution disrupted the cytokinin response and ATP/ADP *ISOPENTENYLTRANSFERASE5* (*AtIPT5*) expression, affecting stem cell initiation and meristem formation. Transcriptomic data suggested that *AUXIN RESPONSE FACTOR3* (*ARF3*) mediated the auxin response during de novo organ regeneration. Indeed, mutations in *ARF3* caused ectopic cytokinin biosynthesis via the misexpression of *AtIPT5*, and this disrupted organ regeneration. We further showed that ARF3 directly bound to the promoter of *AtIPT5* and negatively regulated *AtIPT5* expression. The results from this study thus revealed an auxin-cytokinin cross talk mechanism involving distinct intermediate signaling components required for de novo stem cell initiation and shed new light on the mechanisms of organogenesis in planta.

Plant cells have an amazing capacity to regenerate organs from differentiated somatic tissues under appropriate culture conditions, a process designated de novo organogenesis. De novo organogenesis consists of two steps. The first step involves the formation of the callus, a mass of undifferentiated pluripotent cells derived from various explant tissues grown on callus induction medium (CIM) that has a high auxin-cytokinin ratio. The second involves stem cell initiation, pattern establishment, and organ regeneration. Depending on the auxin-cytokinin ratios of the induction medium, either shoots or roots can be regenerated (Skoog and Miller, 1957; Bhojwani and Razdan, 1996; Che et al., 2002).

Shoot formation is the most studied de novo organogenesis process. Because the shoot meristem gives rise to all aerial parts of the plant body, de novo shoot formation is widely used in agricultural biotechnology to propagate plants. In addition, de novo shoot formation is highly controlled and can thus serve as an excellent experimental system to study fundamental biological processes such as stem cell initiation, cell fate determination, cell differentiation, and hormonal cross talk (Che et al., 2006; Birnbaum and Sánchez Alvarado, 2008).

The formation of the de novo shoot meristem involves a similar degree of patterning and cell organization to that of the embryonic shoot apical meristem (SAM; Mayer et al., 1998; Gordon et al., 2007). The SAM consists of three distinct cell zones: the central zone, the peripheral zone, and the rib zone (Gifford and Corson, 1971; Steeves and Sussex, 1989). At the top of the SAM, the central zone contains stem cells, descendants of which are either displaced to the peripheral zone and

[1] This work was supported by the National Natural Science Foundation of China (grant nos. 91217308, 90917015, and 90717006).

[2] Present address: Key Laboratory of Photosynthesis and Environmental Molecular Physiology, Institute of Botany, Chinese Academy of Sciences, Beijing 100093, China.

* Corresponding author; e-mail zhangxs@sdau.edu.cn.

The author responsible for distribution of materials integral to the findings presented in this article in accordance with the policy described in the Instructions for Authors (www.plantphysiol.org) is: Xian Sheng Zhang (zhangxs@sdau.edu.cn).

[W] The online version of this article contains Web-only data.

[OA] Open Access articles can be viewed online without a subscription.

www.plantphysiol.org/cgi/doi/10.1104/pp.112.203166

may undergo differentiation to form specific organs or to the rib zone to form stem tissues. In addition to a similar cell organization, a common group of regulatory proteins controls the establishment of the shoot meristem both during embryogenesis and de novo organ formation. The expression of *WUSCHEL* (*WUS*) is the earliest event to mark stem cell initiation in Arabidopsis (*Arabidopsis thaliana*). *WUS*-expressing cells in the organizing center establish and maintain stem cell populations within the central zone of the embryonic shoot meristem (Laux et al., 1996; Mayer et al., 1998; Schoof et al., 2000; Weigel and Jürgens, 2002). Ectopic expression of *WUS* is sufficient to induce somatic embryo formation in Arabidopsis (Zuo et al., 2002). Similarly, spatiotemporal *WUS* expression is critical for the establishment of the meristem during de novo shoot formation (Gordon et al., 2007).

Apart from cell organization and a few regulatory proteins such as WUS, little is known about the mechanisms that regulate stem cell initiation and meristem formation during de novo shoot regeneration. Different ratios of exogenous auxin and cytokinin determine cell fates in the callus, indicating the importance of these ratios and the potential cross talk between these two hormones in pattern formation during organ regeneration. Indeed, previous results have shown that the cytokinin response is critical for de novo stem cell initiation and shoot meristem establishment in Arabidopsis (Gordon et al., 2007; Su et al., 2009; Cheng et al., 2010). Mutations of the cytokinin receptor gene *ARABIDOPSIS HISTIDINE KINASE4* (*AHK4*) or type A *ARABIDOPSIS RESPONSE REGULATOR7* (*ARR7*) and *ARR15* affect the de novo shoot formation of Arabidopsis (Buechel et al., 2010). A strong cytokinin response initiated by AHK4 promotes the expression of *WUS*, which is sufficient to induce the formation of the shoot meristem (Gordon et al., 2009). Interestingly, exogenous auxin increases the expression of *AHK4* during callus formation, while exogenous cytokinin regulates the expression of the auxin efflux carriers *PINFORMED* (*PIN*) and the auxin biosynthetic *YUCCA* (*YUC*) genes in the callus (Ruzicka et al., 2009; Jones et al., 2010). In addition, auxin controls cytokinin response through the negative regulation of *ARR7* and *ARR15* by ARF5/MONOPTEROS to maintain SAM (Zhao et al., 2010). The auxin and cytokinin responses transiently and antagonistically interact during early embryogenesis (Müller and Sheen, 2008), suggesting an extensive cross talk between these two hormones during organogenesis.

In this study, we show that a spatiotemporal auxin gradient, established through its coordinated local biosynthesis and polar transport, regulated the spatial cytokinin response during de novo shoot induction. Such an auxin-cytokinin pattern was critical for spatial *WUS* induction, shoot meristem establishment, and subsequent shoot regeneration. We further show that the spatial auxin-cytokinin cross talk was determined by the negative regulation of *ISOPENTENYLTRANSFERASE* genes (in Arabidopsis, *AtIPT*) via the auxin signaling component AUXIN RESPONSE FACTOR3 (ARF3). Our results thus reveal an auxin-cytokinin cross talk for shoot meristem induction that involves novel intermediate signaling components.

RESULTS

Mutually Exclusive Distribution of Auxin and Cytokinin Responses during Stem Cell Initiation and Meristem Formation

Previously, we induced callus formation from plant pistils in an auxin-rich CIM and then transferred the calli onto a cytokinin-rich shoot induction medium (SIM) for shoot induction (Cheng et al., 2010), and we also suggested that the expression of WUS/CLAVATA marked stem cell initiation and that shoot meristem formation is developmentally regulated during these processes (Su et al., 2010). Therefore, we studied the response of endogenous auxin during stem cell initiation and meristem formation using *DR5rev*::*GFP* and *pWUS*::*DsRed-N7* reporter lines. GFP signals were detected uniformly at the edge region of the non-induced callus (SIM0; Fig. 1, A–C). However, these signals progressively translocated to a restrictive region of the outermost cell layers following SIM induction for 2 d (SIM2), when stem cell initiation, as indicated by *WUS* expression, had not yet started (Fig. 1, D–F). SIM induction for 4 d (SIM4) caused relocalization of GFP signals to a "ring" (i.e. a circular region apical and peripheral to the region of high *WUS* expression; Fig. 1, G–N). Formation of shoot meristem by SIM incubation for 6 d (SIM6) accompanied the high GFP signal switch to the region immediately apical to the *WUS* expression domain (Fig. 1, O–R). These results show that the distribution pattern of the auxin response is mutually exclusive of *WUS* expression during stem cell induction and shoot meristem formation.

To evaluate the dynamic distribution of the endogenous cytokinin response during stem cell initiation and meristem formation, we used *TCS*::*GFP* and *pWUS*::*DsRed-N7* reporter lines. *TCS* is a synthetic cytokinin response promoter (Müller and Sheen, 2008). The cytokinin response was distributed to regions corresponding to that of the auxin response in SIM0 (Fig. 2, A–C). However, the cytokinin response adopted a progressively restrictive pattern under SIM induction (Fig. 2, D–F), substantially overlapping with the region of *WUS* expression in SIM4 (Fig. 2, G–M). A strong cytokinin response was detected in a group of cells within the promeristem, overlapping with the *WUS* expression region at SIM6 (Fig. 2, N–Q). These results indicate that the distribution pattern of the cytokinin response overlapped with that of *WUS* expression during stem cell initiation and shoot meristem formation.

To verify the mutually separate distribution of auxin and cytokinin responses during stem cell initiation and

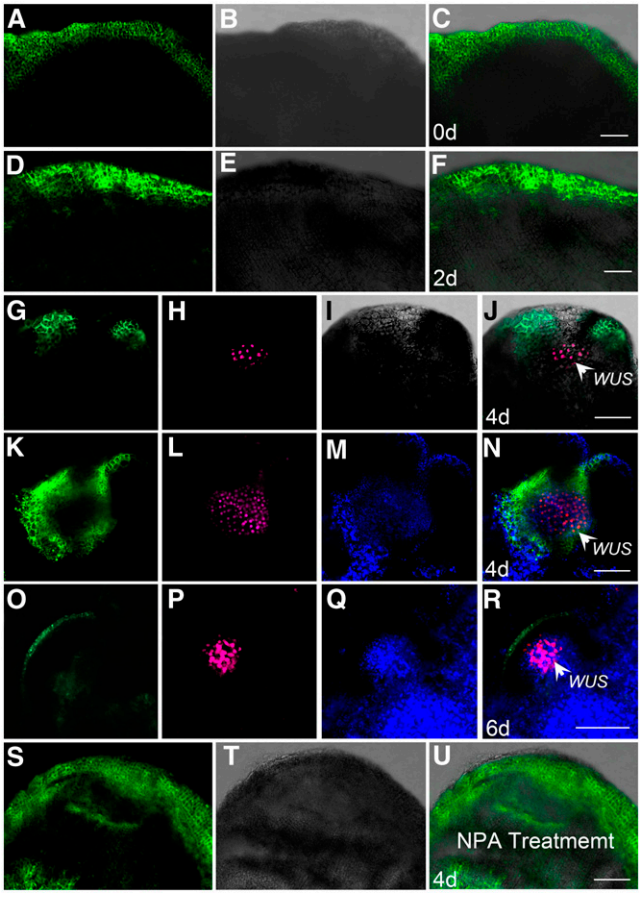

Figure 1. Regional establishment of auxin responses relative to *WUS* expression. A to C, *DR5rev*::*GFP* signals (green) in the edge region of the noninduced callus (SIM for 0 d; 94.3%; $n = 122$). D to F, Regional distribution of *DR5rev*::*GFP* signals in the calli grown on SIM for 2 d (83.3%; $n = 108$). G to J, Auxin distribution indicated by the *DR5rev*::*GFP* signals and *WUS* expression indicated by the *pWUS*::*DsRed-N7* signal (magenta) in calli grown on SIM for 4 d (81.5%; $n = 127$). K to N, Traverse view of the callus grown on SIM for 4 d (80.9%; $n = 110$). O to R, *DR5rev*::*GFP* and *WUS* signals accumulate in the promeristem of calli grown on SIM for 6 d (80.0%; $n = 100$). S to U, Auxin distribution and *WUS* expression in the calli grown on NPA-containing SIM for 4 d (86.8%; $n = 152$). Bright-field (B, E, I, and T) and merged images of GFP (green) and DsRed (magenta) channels (J, N, and R) are shown. Chlorophyll autofluorescence is shown in blue (M, N, Q, and R). Bars = 100 μm.

shoot meristem formation, we performed double labeling using reporter lines expressing both *TCS*::*GFP* and *DR5rev*::*3XVENUS-N7*. The cytokinin and auxin responses merged well at the edge region at SIM0 (Supplemental Fig. S1A), as shown by separate labeling experiments (Figs. 1, A–C, and 2, A–C). However, SIM4 resulted in translocation of the *DR5rev* signals to the "auxin ring" region, whereas the cytokinin response was restricted to the center of the auxin ring (Supplemental Fig. S1, B and C), where *WUS* expression was also detected (Fig. 2, G–I). These results show that the auxin response is distinct from the cytokinin response, which is associated with the *WUS* expression pattern during stem cell initiation and shoot meristem induction, demonstrating a mutually exclusive distribution of the auxin and cytokinin responses during these processes.

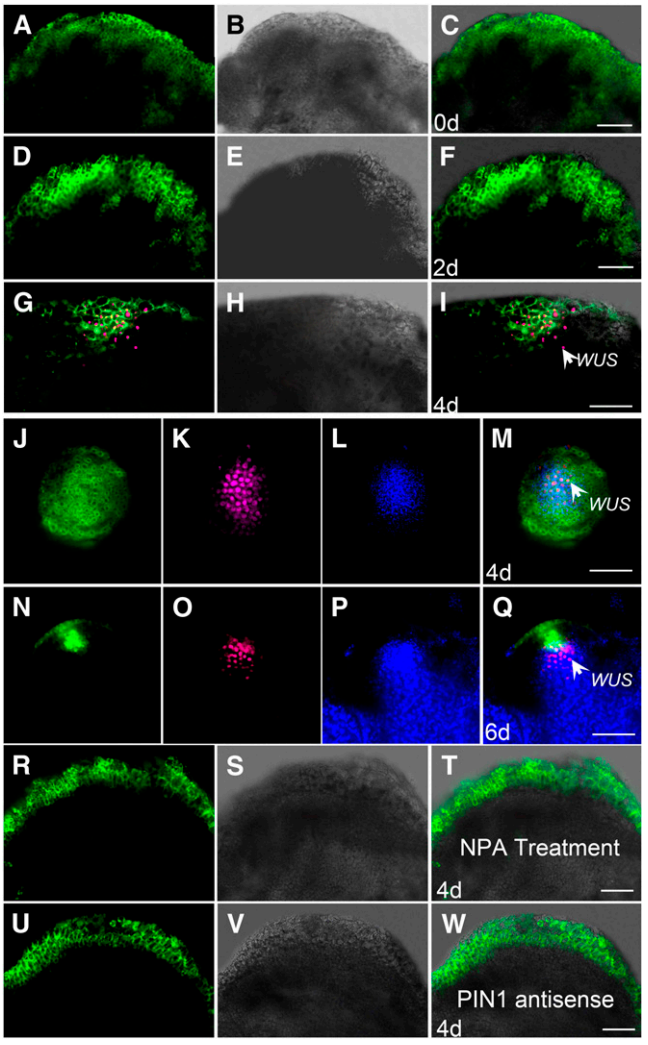

Figure 2. Regional establishment of cytokinin responses relative to *WUS* expression. A to C, *TCS*::*GFP* signals (green) in the edge of the noninduced callus (94.5%; $n = 127$). D to F, *TCS*::*GFP* signals beginning to distribute regionally in the calli grown on SIM for 2 d (85.9%; $n = 128$). G to I, Regional distribution of the *TCS*::*GFP* signals colocalizes with the *pWUS*::*DsRed-N7* signal (magenta) in the calli grown on SIM for 4 d (89.2%; $n = 222$). J to M, Traverse views of the calli grown on SIM for 4 d. N to Q, *TCS*::*GFP* and *WUS* signals accumulated in the promeristem of calli grown on SIM for 6 d (80.0%; $n = 110$). R to T, Cytokinin response (*TCS*::*GFP*) and *WUS* (*pWUS*::*DsRed-N7*) expression in the callus grown on NPA-containing SIM for 4 d. U to W, Cytokinin responses (*TCS*::*GFP*) in the calli transformed with antisense *PIN1* driven by an estrogen receptor-based transactivator, XVE (for fusion of the DNA-binding domain of the bacterial repressor LexA, the acidic trans-activating domain of VP16, and the regulatory region of the human estrogen receptor). The calli were incubated on estrogen-containing SIM for 4 d (82.8%; $n = 116$). A to I and N to W are longitudinal sections of calli. Bright-field (B, E, H, S, and V) and merged images of GFP (green) and DsRed (magenta) channels (I, M, and Q) are shown. Chlorophyll autofluorescence is shown in blue (L, M, P, and Q). Bars = 100 μm.

The Spatiotemporal Auxin Response Contributed by Local Auxin Biosynthesis and Auxin Transport Plays Important Roles in de Novo Shoot Regeneration

Because the regional auxin response could be the result of local auxin biosynthesis or dynamic auxin transport, we studied these two aspects during de novo shoot formation. A major pathway leading to auxin biosynthesis is mediated by the YUCs (Cheng et al., 2006). Using genome-wide transcriptional and quantitative reverse transcription (qRT)-PCR analyses, we found that the transcriptional levels of *YUC1* and *YUC4* among the *YUC* members were significantly enhanced during shoot induction (Fig. 3A; Li et al., 2011; ArrayExpress accession no. E-MEXP-3120). Furthermore, we observed that SIM4 greatly induced the promoter activity of the *pYUC1*::*GUS* and *pYUC4*::*GUS* reporter lines, for which GUS activity was restricted to the future shoot initiation sites by SIM4, whereas no GUS activity was detected on SIM0 (Fig. 3, B and C). Time-lapse analysis of reporter lines containing both *pYUC4*::*GFP* and *pWUS*::*DsRed-N7* showed a similar dynamic distribution of *YUC4* promoter activity to that of the auxin response, neither of which overlapped with the *WUS*-expressing region on SIM4 (Figs. 1, G–N, and 3, E–G). These results suggest that *YUC1*- and *YUC4*-mediated auxin biosynthesis contributes to the distribution of the auxin response.

With the exception of auxin biosynthesis, polar auxin transport via auxin efflux carrier PINs may also contribute to the spatially restricted auxin distribution (Wiśniewska et al., 2006). Indeed, although PIN1 did not show polarized membrane localization at SIM0 (Supplemental Fig. S2, A–C), SIM incubation for 1 d (SIM1) induced its polarization (Supplemental Fig. S2, D–F). Prolonged incubation on SIM resulted in a more restricted and polarized localization pattern (Supplemental Fig. S2, G–I). At SIM4, PIN1 was detected in the outermost cell layer of the region apical to that of the *WUS* expression domain where stem cells would be initiated (Supplemental Fig. S2, J–Q). At SIM6, PIN1 became accumulated in the cells of layer 1 of the promeristem (Supplemental Fig. S2, R–U). To provide further evidence of whether PIN1-mediated polar auxin transport is critical for the auxin response during stem cell initiation and shoot meristem formation, we undertook pharmacological analysis using *N*-1-naphthylphthalamic acid (NPA), an inhibitor of polar auxin transport (Lomax et al., 1995). The application of NPA at SIM4 disrupted the spatiotemporal auxin response and *WUS* expression (Fig. 1, S–U) in a manner that resembled the situation in the noninduced callus (Fig. 1, A–C).

The spatiotemporal expression of both the auxin biosynthetic and auxin transport pathways correlated well with the distribution of the auxin response during de novo shoot regeneration. To test whether this correlation is biologically relevant, we analyzed the efficiencies of the de novo shoot regeneration of plants whose auxin biosynthesis or polar transport mechanisms had been genetically disrupted. As shown in Table I, mutations of both *YUC1* and *YUC4* caused significantly lower regeneration frequencies than the wild type or *YUC* single mutants (Supplemental Table S1). The frequency of shoot regeneration was significantly reduced by expressing antisense *PIN1* (Table I). These results indicate that the genetic disruption of either auxin biosynthesis or polar auxin transport suppresses shoot regeneration, further indicating the importance of the auxin response during de novo shoot regeneration.

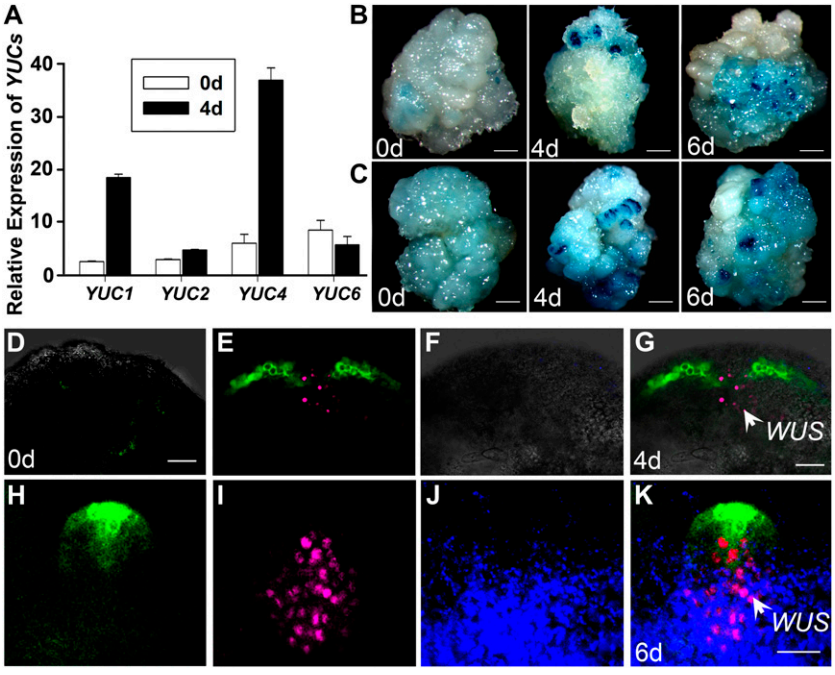

Figure 3. Spatiotemporal expression of auxin biosynthetic genes during shoot induction. A, qRT-PCR analysis of *YUC* expression level in noninduced calli and in calli grown on SIM for 4 d. B, *pYUC1*::*GUS* signals in noninduced calli (91.7%; $n = 121$) and in calli grown on SIM for 4 d (84.0%; $n = 156$) or 6 d (81.5%; $n = 162$). C, *pYUC4*::*GUS* signals in the noninduced callus (85.9%; $n = 198$) and in the calli grown on SIM for 4 d (85.6%; $n = 167$) or 6 d (83.3%; $n = 150$). D to K, Localization of *pYUC4*::*GFP* (green) and *pWUS*::*DsRed-N7* (magenta) signals in the noninduced callus (D; 90.2%; $n = 122$) and in calli grown on SIM for 4 d (E–G; 84.4%; $n = 166$) or 6 d (H–K; 80.3%; $n = 152$). D to K are longitudinal sections of calli. Bright-field (D and F) and merged images of GFP (green) and DsRed (magenta) channels (G and K) are shown. Chlorophyll autofluorescence is shown in blue (J and K). Bars = 1 mm (B and C) and 100 μm (D, G, and K).

Table I. *Mutations in auxin- and cytokinin-related genes alter the rate of Arabidopsis shoot regeneration in vitro using pistils as explants*

For the measurement of shoot regeneration frequencies from wild-type and mutant calli, calli cultured on SIM for 14 d were used. Data are mean values from three sets of biological replicates. In each replicate, at least 100 calli were examined.

Mutants and Antisense *PIN1*	Regeneration Frequency
	%
Wild type (ecotype Col)	24.36 ± 1.11
yuc1 single mutant (ecotype Col)	23.98 ± 1.22[a]
yuc2 single mutant (ecotype Col)	22.65 ± 1.13[a]
yuc4 single mutant (ecotype Col)	22.68 ± 1.60[a]
yuc6 single mutant (ecotype Col)	23.57 ± 1.24[a]
yuc1 yuc4 double mutant (ecotype Col)	9.21 ± 0.89[b]
arf1 single mutant (ecotype Col)	23.26 ± 1.91[a]
Wild type (ecotype Ws)	88.26 ± 2.13
arf3/ett-1 single mutant (ecotype Ws)	7.90 ± 1.14[b]
arf3/ett-2 single mutant (ecotype Ws)	35.58 ± 2.07[b]
Antisense *PIN1* cDNA (ecotype Ws)	7.63 ± 1.46[b]
atipt5 single mutant (ecotype Ws)	79.86 ± 1.14[a]
Wild type (ecotype Col × Ws)	80.86 ± 1.34
atipt5,7 double mutant (ecotype Col × Ws)	43.34 ± 2.02[b]
atipt3,5,7 triple mutant (ecotype Col × Ws)	6.44 ± 1.30[b]

[a]Not significantly different from the wild type (Student's *t* test, $P > 0.05$). [b]Significantly different from the wild type (Student's *t* test, $P < 0.01$).

The Spatiotemporal Biosynthesis of Cytokinin Relies on Polar Auxin Transport

Because the cytokinin response, as indicated by *TCS*::*GFP* reporter signals, showed a spatially restricted distribution in the callus following SIM incubation (Fig. 2, A–M), we wondered whether this resulted from cytokinin biosynthesis. To test this possibility, we analyzed the expression of the cytokinin biosynthetic *AtIPT* genes by qRT-PCR. The expression of *AtIPT3*, *AtIPT5*, and *AtIPT7* was up-regulated in SIM incubation (Fig. 4A). Using the *pAtIPT5*::*GUS* reporter line, we detected the expression of *AtIPT5* at the whole edge of the noninduced callus (Fig. 4, B and F). Incubation on SIM caused a gradual disappearance of the *AtIPT5* signals in all regions except those of the future promeristems (Fig. 4, C, D, and G). Eventually, the *AtIPT5* signals were restricted to the promeristem region (Fig. 4, E and H). In addition, mutations of the *AtIPTs* significantly reduced the frequencies of shoot regeneration. Shoot regeneration frequencies of the *atipt5 atipt7* double mutants and the *atipt3 atipt5 atipt7* triple mutants were much lower than those of the wild type or single mutants (Table I). These molecular and genetic analyses indicate the importance of *AtIPT*-dependent cytokinin biosynthesis during de novo shoot regeneration.

Because the cytokinin response was spatially correlated with the auxin response (Figs. 1, A–C, and 2, A–C), we tested whether interrupting the auxin response pathway could affect the dynamic cytokinin response. For this hypothesis, we disrupted the polar auxin transport of the *TCS*::*GFP* reporter lines either genetically by down-regulating *PIN1* expression or pharmacologically by applying NPA. Both *PIN1* down-regulation and NPA treatment abolished the dynamic distribution of cytokinin response initiated by SIM induction (Fig. 2, R–W). NPA treatment also abolished SIM-induced *WUS* expression (Fig. 2, R–T). In addition, NPA treatment abolished the translocation of *AtIPT5* expression during SIM induction (Fig. 4, I–K). These data indicate that the distribution of the cytokinin response and cytokinin biosynthesis depend on polar auxin transport and, by inference, on an intact auxin response.

ARF3 Mediates the Auxin Response during de Novo Shoot Regeneration

Genetic and pharmacological evidence has revealed the importance of the auxin response during de novo

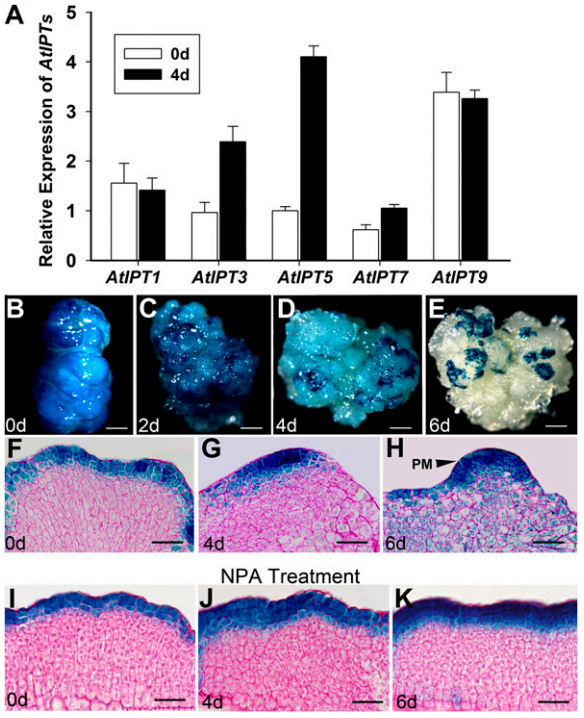

Figure 4. Expression of cytokinin biosynthetic *AtIPT* genes within the callus during shoot induction and following NPA treatment. A, Expression levels of *AtIPTs* in the noninduced calli and in calli grown on SIM for 4 d determined by qRT-PCR. B, *pAtIPT5*::*GUS* signals in the noninduced callus (85.9%; $n = 199$). C to E, Regional distribution of *pAtIPT5*::*GUS* signals in calli grown on SIM for 2 d (C; 90.5%; $n = 199$), 4 d (D; 89.5%; $n = 190$), or 6 d (E; 87.9%; $n = 182$). F to H, *AtIPT5* expression patterns in the noninduced callus (F; 90.9%; $n = 209$) and in calli grown on SIM for 4 d (G; 89.5%; $n = 190$) or 6 d (H; 87.9%; $n = 182$). I to K, *pAtIPT5*::*GUS* signals distributed uniformly at the edge region of the calli grown on SIM for 0 d (I; 85.2%; $n = 88$), 4 d (J; 83.3%; $n = 66$), and 6 d (K; 84.9%; $n = 63$) when treated with NPA. F to K are longitudinal sections of calli. PM, Promeristem. Bars = 700 μm (B–E), 200 μm (F, G, I, and J), and 50 μm (H).

shoot regeneration. To evaluate whether there are changes at the auxin level during de novo shoot regeneration, we assayed the endogenous auxin concentration during shoot induction. The auxin level was significantly higher in the calli of SIM4 when stem cell initiation and meristem formation had commenced than that of SIM0 when only nondifferentiating pluripotent cells were present (Supplemental Fig. S3). The increased auxin level was correlated with an increased expression of auxin biosynthetic genes (Fig. 3A).

The increased endogenous auxin level following SIM induction prompted us to identify the auxin response genes that might function in de novo shoot regeneration. To this end, we performed genome-wide transcriptomic analysis using the Affymetrix Arabidopsis ATH1 Genome Arrays (Li et al., 2011; Supplemental Table S2; ArrayExpress accession no. E-MEXP-3120). Among the genes whose transcriptional change from SIM0 to SIM4/SIM6 were more than 1.5-fold, we identified several *ARFs* (Supplemental Table S2). However, *ARF3* was the only gene in our data set that appeared to be up-regulated by SIM incubation in a previous transcriptomic screen when the roots were used as explants (Che et al., 2006).

Exogenous auxin was found to up-regulate *ARF3* expression (Supplemental Fig. S4). To elucidate the expression pattern of *ARF3* during shoot regeneration, we performed in situ hybridization. The *ARF* signals were distributed evenly at the edge region of the SIM0 callus (Fig. 5A). SIM2 caused a spatial restriction of *ARF3* expression (Fig. 5B). Progressive translocation of *ARF3* expression by SIM incubation resulted in a pattern (Fig. 5, C and D) similar to that of the auxin response (Fig. 1, G–N). Finally, high *ARF3* expression was detected in the shoot meristem (Fig. 5E). These results show that the *ARF3* expression profile parallels the dynamic auxin response distribution during shoot meristem formation.

To test whether *ARF3* mediates the auxin response during de novo shoot regeneration, we adopted a reverse genetic approach. Using two mutant alleles for *ARF3*, *arf3/ett-1*, a null mutant, and *ett-2*, a weak mutant (Sessions et al., 1997; Sohlberg et al., 2006), we first compared the frequencies of de novo shoot regeneration of the mutants versus the wild type. As shown in Table I, mutations of *ARF3* caused a significant reduction of shoot regeneration. Consistent with the properties of the two *ARF3* mutants, the strong allele *ett-1* hardly regenerated any shoots while the weak allele *ett-2* showed some shoot regeneration capacity, although much reduced compared with the wild type (Table I; Fig. 5, F–H). We also determined the frequency of shoot regeneration in the *ett-1 atipt5-1* double mutant. The result showed that the double mutant, with 12.85% ± 2.56%, was slightly lower than the *ett-1* single mutant, with 16.67% ± 1.06% (Supplemental Fig S5). Because ARF3 is considered to be a transcriptional repressor (Guilfoyle and Hagen, 2007), we further tested the shoot regeneration frequencies of other ARFs that also serve as transcriptional repressors. However, none of the other repressor ARFs affected the frequencies of de novo shoot regeneration (Table I; Supplemental Table S1), consistent with our transcriptomic data, in which none of the other repressor *ARFs* showed significant transcriptional changes (Supplemental Table S2). These results indicate that ARF3 is a key mediator of the auxin response during de novo shoot regeneration.

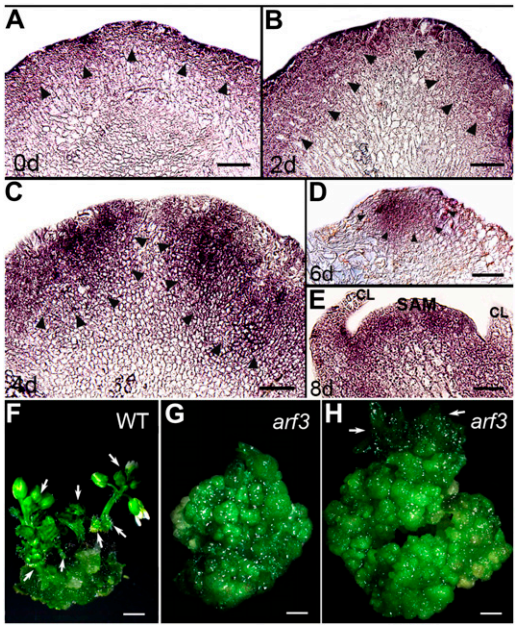

Figure 5. Spatiotemporal expression of *ARF3* and its mutational effects on shoot formation. A to E, In situ hybridization analyses showing the spatial expression of *ARF3* in the noninduced callus (A; 87.5%; n = 112) or in calli grown on SIM for 2 d (B; 80.5%; n = 123), 4 d (C; 75.4%; n = 130), 6 d (D; 72.7%; n = 110), or 8 d (E; 73.2%; n = 123). F, Regenerated shoots from wild-type (WT) calli grown on SIM for 18 d (89.9%; n = 99). G, The *arf3/ett2* mutant callus grown on SIM for 18 d showing no shoot regeneration. H, The *arf3/ett2* mutant callus grown on SIM for 18 d with a few regenerated shoots (34.5%; n = 200). CL, Cauline leaf. Arrows indicate regenerated shoots, and arrowheads indicate *ARF3* signals. A to E are longitudinal sections of calli. Bars = 100 μm (A–C), 50 μm (D and E), and 1 mm (F–H).

ARF3 Negatively Regulates Spatiotemporal *AtIPT* Expression

Disrupting polar auxin transport abolished the dynamic cytokinin response induced by SIM (Fig. 2, R–W), suggesting that the SIM-induced cytokinin response is dependent on auxin signaling. Because ARF3 mediates the auxin response to SIM induction and the dynamic cytokinin response results from *AtIPT* expression, we used several approaches to test whether these two pathways converge.

First, we analyzed the GUS pattern of *pAtIPT5*::*GUS* reporter lines either in the wild type or the *arf3/ett-2* mutant background to detect possible changes in *AtIPT5* expression. We did not observe any difference in the

GUS staining patterns at SIM0 between the wild type and the *arf3* mutants (Fig. 6, A and C). However, GUS signals were found to be restricted to the future promeristem region by SIM4 in the wild type (Fig. 6B) but to be insensitive to SIM induction in the *arf3* mutants (Fig. 6D). In addition, the transcript levels of *AtIPT5* were increased in the *arf3* single mutants compared with the wild-type lines under SIM induction (Fig. 7). These data suggest that ARF3 negatively regulates *AtIPT5* expression in high-auxin-response regions.

Second, we evaluated the effects of mutating the auxin response elements (AuxREs) within the promoter sequence of *AtIPT5* and found that they rendered this gene insensitive to SIM induction in the wild-type background. AuxREs, including three TGTCTC elements and 13 TGTCNN elements (Ulmasov et al., 1999a), were identified within a 2.2-kb promoter region of *AtIPT5* (Fig. 6E; Supplemental Table S3). We generated a mutant version of the *AtIPT5* promoter (*AtIPT5m*) that contained point mutations in several AuxREs potentially abolishing ARF binding (Fig. 6E). The GUS activity of the *pAtIPT5m*::*GUS* reporter line showed a similar uniform distribution pattern (Fig. 6F) to that of the *pAtIPT5*::*GUS* reporter line at SIM0 (Fig. 6A). However, the GUS activity of the *pAtIPT5m*::*GUS* reporter line failed to respond to SIM induction, and the spatial restriction of the reporter activity normally observed in the *AtIPT5*:*GUS* line did not occur (Fig. 6G).

To test whether ARF3 directly binds to the promoter of *AtIPT5*, we performed yeast one-hybrid analysis, surface plasmon resonance (SPR) measurements, and electrophoretic mobility shift assays (EMSAs). The yeast one-hybrid experiments showed growth of the yeast on selection medium, suggesting positive binding of ARF3 to the *AtIPT5* promoter (Fig. 8A). Furthermore, ARF3 proteins were produced by in vitro transcription and translation and were used in SPR and EMSA analyses (Supplemental Table S3). Elevated resonance unit values were detected over time (Fig. 8B). In EMSA experiments using biotin-labeled 26-bp oligonucleotides (−155 to −130) covering two AuxREs, a clear ARF3-dependent mobility shift was identified (Fig. 8C). The wild-type oligonucleotides could compete for binding of the ARF3 proteins, whereas the mutated oligonucleotides for the AuxREs could not (Fig. 8C), indicating that ARF3 proteins directly bind to the promoter region of *AtIPT5* to regulate its expression (Supplemental Table S3).

To next determine whether ARF3 directly associates with the promoter sequence of *AtIPT5* in vivo, we performed chromatin immunoprecipitation (ChIP) assays using the *pARF3*::*ARF3tasiR-GUS* transgenic lines (Columbia [Col]; Marin et al., 2010). As shown in Figure 8E, compared with the mouse IgG mock control, the calli sampled from *pARF3*::*ARF3tasiR-GUS* transgenic lines showed a strong enrichment of fragment a (covering −155 to −130 in EMSA) but not of fragment b (negative control) in the promoter region (Fig. 8, D and E). Fragment a was moderately enriched in calli sampled from *pMP* (*ARF5*)::*MP-GFP* transgenic plants and was not enriched at all in *35S*::*6myc-ARF8* transgenic calli (Fig. 8E). These results indicate that ARF3 proteins directly bind to the promoter of *AtIPT5* in vivo.

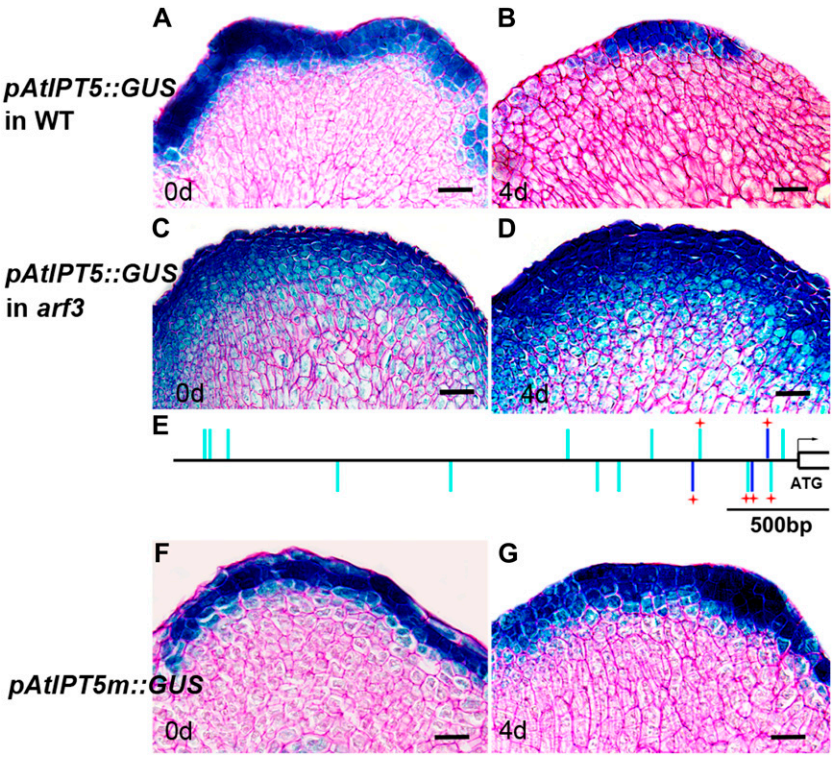

Figure 6. AuxRE-dependent ectopic expression of *AtIPT5* in *arf3*. A and B, *pAtIPT5*::*GUS* signals in the wild-type callus induced on SIM for 0 d (A; 89.5%; $n = 190$) or 4 d (B; 85.9%; $n = 199$). C and D, GUS signals in the calli of the *arf3* mutant grown on SIM for 0 d (C; 82.7%; $n = 168$) or 4 d (D; 80.4%; $n = 148$). E, Schematic illustration of the *AtIPT5* promoter. TGTCTC and TGTCNN on both the sense and antisense strands are indicated by blue and green bars, respectively; red plus signs denote point mutations (TGTC→TGGC). F and G, *pAtIPT5m*::*GUS* signals in the noninduced callus (F; 88.8%; $n = 179$) or in the calli grown on SIM for 4 d (G; 85.4%; $n = 198$). A to D, F, and G are longitudinal sections of calli. Bars = 80 μm.

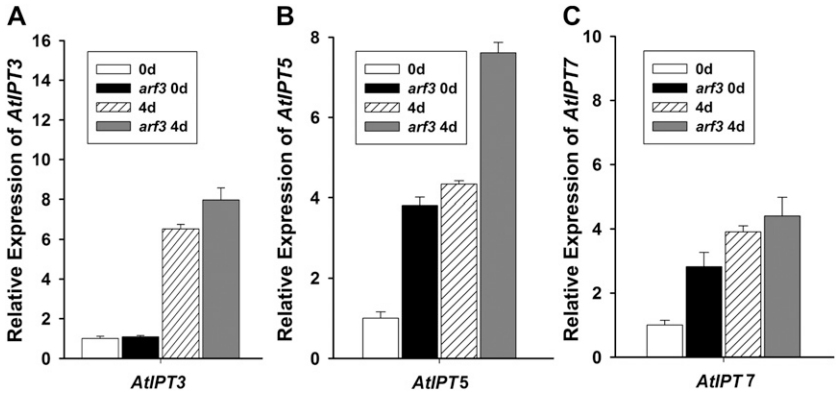

Figure 7. *AtIPT* expression is enhanced in the *arf3* mutant. qRT-PCR analyses show that the expression of *AtIPT3* (A), *AtIPT5* (B), and *AtIPT7* (C) was enhanced in the *arf3* mutant. *AtIPT5* was the most significantly enhanced under these conditions.

DISCUSSION

Plant tissues could regenerate shoots or somatic embryos in vitro, two processes that could be mechanistically distinct (Verdeil et al., 2007). Shoot regeneration reflects cell pluripotency, while somatic embryo induction is the full expression of totipotency (Verdeil et al., 2007; Atta et al., 2009). Previously, we showed that auxin response signals did not accumulate at the edge region of embryonic callus before somatic embryo induction (Su et al., 2009). However, strong signals were evenly distributed at the edge region of callus before shoot meristem induction (Fig. 1, A–C). This difference implies that although auxin plays important roles in both processes, organ regeneration and somatic embryogenesis are regulated by different mechanisms.

Auxin has been proposed to be a morphogen in planta (Dubrovsky et al., 2008) due to its versatility in plant development (Vanneste and Friml, 2009), including meristem formation and embryogenesis (Reinhardt et al., 2000; Heisler et al., 2005; Müller and Sheen, 2008). Auxin signaling extensively interplays with the signal responses of other phytohormones, such as cytokinin, brassinosteroid, and ethylene (Ruzicka et al., 2009; Jones et al., 2010; Depuydt and Hardtke, 2011; Willige et al., 2011). Exogenous auxin represses local cytokinin biosynthesis in the nodal stem of pea (*Pisum sativum*) through *PsIPT1* and *PsIPT2* (Tanaka et al., 2006). Cytokinin biosynthesis during organogenesis was also found to be negatively regulated by auxin treatment (Nordström et al., 2004). In developing root and shoot tissues, ectopic biosynthesis of cytokinin causes a rapid increase in auxin biosynthesis (Jones et al., 2010). Cytokinin also alters auxin responses through the transcriptional regulation of auxin signaling and transport-related genes (Dello Ioio et al., 2008; Ruzicka et al., 2009). However, the underlying molecular mechanisms between auxin and cytokinin interaction during shoot induction remain unknown.

We showed here that auxin response controlled the spatiotemporal distribution of cytokinin biosynthesis through the negative regulation of *AtIPT* expression by ARF3 during de novo shoot regeneration. Previous studies have reported that auxin biosynthesis (Cheng et al., 2007; Zhao, 2008) and polar transport (Wiśniewska et al., 2006) can occur spatiotemporally. As a result, auxin signaling is location sensitive (Weijers et al., 2006; Schlereth et al., 2010). We also showed that the auxin response was promoted by exogenous cytokinin through local auxin biosynthesis and polar auxin transport, resulting in the formation of the auxin ring within the callus where cytokinin biosynthesis was inhibited. The spatiotemporal biosynthesis of cytokinin could then be sensed by AHK4 to promote local *WUS* expression, leading to stem cell initiation and meristem formation (Gordon et al., 2009; Su et al., 2011). Our results here thus reveal a novel molecular mechanism that underlies auxin-cytokinin cross talk. Such a cross talk plays a critical role in stem cell initiation and meristem formation during de novo shoot regeneration.

Some crucial questions remain to be addressed. First, it is necessary to point out that ARF3 is an atypical ARF, lacking two domains for dimerization with the auxin/indole-3-acetic acids, whereas dimerization with and the auxin-induced degradation of auxin/indole-3-acetic acids is the standard auxin-sensing mechanism for ARFs (Ulmasov et al., 1999a; Guilfoyle and Hagen, 2007). Hence, ARF3 either senses auxin signals through cofactors, as reported previously (Ulmasov et al., 1999a; Pfluger and Zambryski, 2004), or utilizes a yet-to-be-identified mechanism for auxin sensing. Second, it has been shown that activator-type ARFs and repressor-type ARFs can bind to the same AuxREs and thus regulate the same target genes (Ulmasov et al., 1999b; Vernoux et al., 2011). The ARF activator-to-repressor ratio is critical for the stability of gene expression during auxin response (Vernoux et al., 2011). Our results showed that both the repressor ARF3 and the activator ARF5 bound to the promoter of *AtIPT5* (Fig. 6E). This result put forward the interesting possibility that ARF3 and ARF5 antagonistically regulated the expression of *AtIPT5*, a possibility worthy of further analysis. Third, de novo stem cell initiation and meristem formation are induced by SIM containing high cytokinin and low auxin (Skoog and Miller, 1957). High cytokinin levels could regulate the

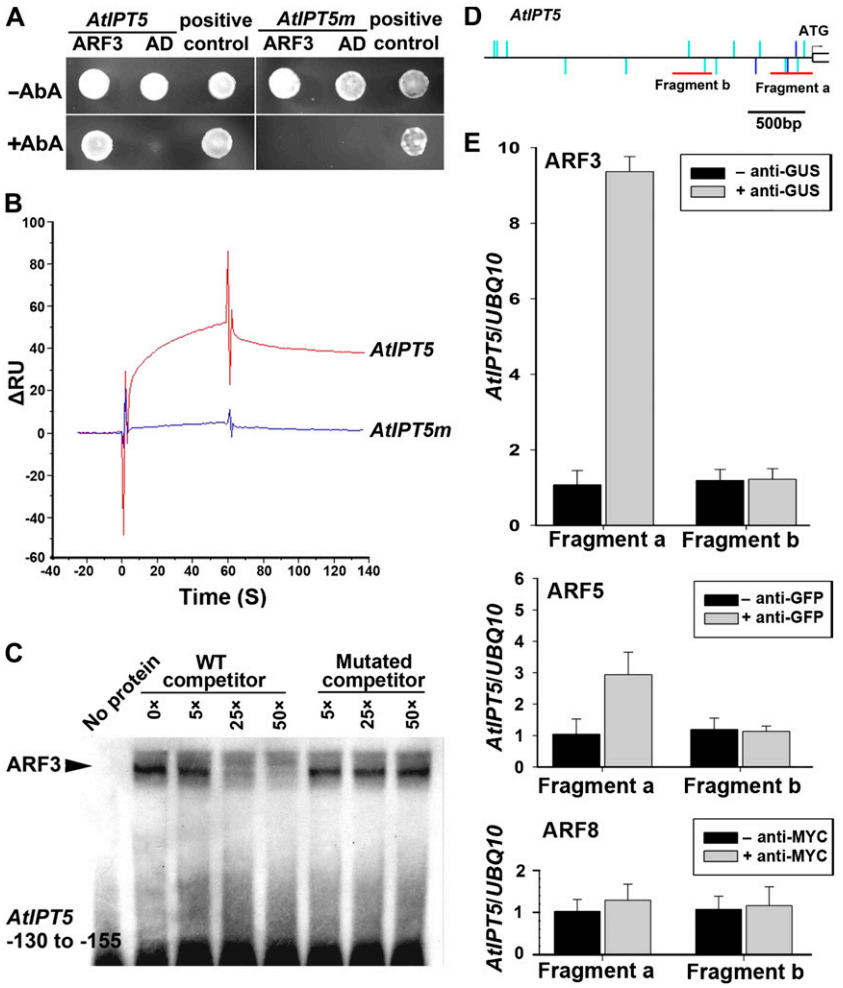

Figure 8. ARF3 directly binds to the promoter of *AtIPT5*. A, Yeast one-hybrid analysis revealing the direct interaction between ARF3 and the *AtIPT5* promoter. Yeast strains containing the PAtIPT5 promoter-AbAi or PAtIPT5m promoter-AbAi construct were grown on medium under selective (SD/−Leu; +100 ng mL^{-1} AbA) or nonselective (SD/−Leu; −AbA) conditions. Full-length *ARF3* cDNAs fused to pGADT7 AD are indicated on the plates, and the empty pGADT7 AD vector was used as a negative control. The p53-AbAi vector was used as a positive control in the kit (Clontech Laboratories). B, Interaction between ARF3 and the *AtIPT5* promoter (red line) was determined by SPR analysis. The *AtIPT5m* promoter was introduced as a negative control (blue line). C, EMSA analysis showing the interaction between ARF3 and the *AtIPT5* promoter. The retarded DNA-protein complex was competed using either wild-type (WT) probe or the mutated probes at a 5×, 25×, or 50× molar excess. D, The AuxREs TGTCTC and TGTCNN on both sense and antisense strands of the *AtIPT5* promoter are indicated as blue and green bars, respectively. Red lines indicate fragments amplified in E. Fragment a (−356 to +39) includes the sequence used in the EMSA experiments (−155 to −130), and fragment b (−1,133 to −850) was used as a negative control. E, Enrichment of specific regions of the *AtIPT5* promoter (fragments a and b) using anti-GUS, anti-GFP, and anti-MYC antibodies in *pARF3*::*ARF3tasiR-GUS*, *pMP*(*ARF5*)::*MP-GFP*, and *35S*::*6myc-ARF8* transgenic plants, respectively. Mouse IgG was used as a mock control. The fold enrichments of specific regions (fragments a and b) were detected by qRT-PCR analysis after normalization to the unrelated *UBQ10* control sequence. Means were calculated from three biological replicates, and each biological sample was examined using three PCR technical replicates.

expression of the auxin biosynthetic *YUC* genes or the polar auxin transporter *PINs*, as reported in planta (Ruzicka et al., 2009; Jones et al., 2010). However, except for *ARF3*, whose expression was induced by exogenous cytokinin, no other target genes transcriptionally responding to cytokinin in callus was identified. Genes identified by SIM induction in our transcriptomic data might contain such candidates.

Taken together, we propose that the specific pattern of auxin-controlled cytokinin distribution determines the developmental fate of pluripotent cells during de novo SAM formation. Auxin biosynthesis and transport mediate the local auxin response, which defines the spatial distribution of cytokinin. Such a cross talk is mediated through the negative regulation of *AtIPTs* by ARF3, possibly together with other ARFs. This

spatiotemporal distribution of cytokinin is essential for *WUS* induction, which controls meristem formation (Gordon et al., 2009). Our study thus provides new and important findings on the molecular mechanisms underlying de novo shoot regeneration.

MATERIALS AND METHODS

Plant Materials and Growth Conditions

Arabidopsis (*Arabidopsis thaliana*) ecotypes Wassilewskija (Ws) and Col were used in this study. Marker lines of the Col and Landsberg *erecta* ecotypes were crossed with wild-type Ws for at least four generations to clear the genetic background. The origins and ecotypes of the transgenic lines and mutants were as follows: *pWUS*::*DsRed-N7* and *DR5rev*::*3XVENUS-N7* (Landsberg *erecta*; Gordon et al., 2007); *DR5rev*::*GFP* and *pPIN1*::*PIN1-GFP* (Col; Xu et al., 2006); *pAtIPT5*::*GUS* (Ws; Atta et al., 2009); *pARF3*::*ARF3tasiR-GUS* (Col; Marin et al., 2010); *pMP* (*ARF5*)::*MP-GFP* (Col; Schlereth et al., 2010); *pYUC1*::*GUS*, *pYUC4*::*GUS*, the single mutants *yuc1*, *yuc2*, *yuc4*, and *yuc6*, and the double mutants *yuc1 yuc4* (Col; Cheng et al., 2007); the single mutant *arf4-1* (Col; Pekker et al., 2005); the single mutants *atipt5-1* (Ws) and *atipt7-1* (Col), the double mutants *atipt5-1 atipt7-1*, and the triple mutants *atipt3-2 atipt5-1 atipt7-1* (Miyawaki et al., 2006); and antisense *PIN1* vectors (Ws; Su et al., 2009). The single mutants *arf3* (*ett-2*; CS8555; Ws ecotype), *arf1-2* (CS24598; Col ecotype), and *arf9-1* (CS24609; Col ecotype) were obtained from the Arabidopsis Biological Resource Center. The *arf3* (*ett-1*; Ws ecotype) single mutants were kindly provided by Sohlberg et al. (2006). The *TCS*::*GFP* construct (Müller and Sheen, 2008) was previously transformed into wild-type (Ws) plants that harbor *pWUS*::*DsRed-N7* using the *Agrobacterium tumefaciens*-mediated floral dip method (Clough and Bent, 1998).

Seeds were sterilized and plated on 0.8% (w/v) agar solid medium (one-half-strength Murashige and Skoog, 0.5% [w/v] Suc, pH 5.7; Murashige and Skoog, 1962). After cold treatment to overcome dormancy, they were cultivated under sterile conditions (light intensity of 40 μmol photons m^{-2} s^{-1}, 20°C–22°C, with a 16-h-light/8-h-dark cycle) for approximately 35 d as explants.

In Vitro Culture and Shoot Induction

In vitro culture and shoot induction using pistils as explants were performed according to Cheng et al. (2010).

Construction of GFP and GUS Reporters

For the *pYUC4*::*GFP* construct, a DNA fragment containing a 2,873-bp sequence upstream of the translational start codon of *YUC4* was subcloned in the pBI121-GFP vector. The primers *YUC4*p-F and *YUC4*p-R are listed in Supplemental Table S4. For the *pAtIPT5m*::*GUS* construct, a DNA fragment containing 2,019 bp of mutated sequence upstream of the translational start codon of *AtIPT5* was subcloned in the pBI121-GUS vector. The primers *PAtIPT5*-F, *PAtIPT5*-R, *PAtIPT5A*-F, *PAtIPT5A*-R, *PAtIPT5B*-F, *PAtIPT5B*-R, *PAtIPT5C*-F, *PAtIPT5C*-R, *PAtIPT5D*-F, and *PAtIPT5D*-R are also listed in Supplemental Table S4.

GUS Assays

GUS assays were performed as described previously by Cheng et al. (2010).

In Situ Hybridization

Plant tissues were fixed in 10% formaldehyde, 5% acetic acid, and 50% alcohol overnight at 4°C. After dehydration, the fixed tissues were embedded in Paraplast (Sigma) and sectioned at 8 μm. Antisense and sense RNA probes were used for hybridization according to a detailed process described previously by Zhao et al. (2006). The sequences of the ARF3-F and ARF3-R probes are listed in Supplemental Table S4.

Confocal Microscopy

Approximately 100 calli were imaged to determine the patterns of each marker at different time points after induction. Light-yellowish calli of approximately 3 to 5 mm in diameter were selected using an Olympus JM dissecting microscope and then cut into 1- to 2-mm sections along the longitudinal axis of the callus. These sections were observed, and all fluorescence images were captured using a confocal laser scanning microscope (Zeiss 510 Meta CLSM device with 10× air, 20× air, 40× oil, and 63× oil objectives). For colabeling by VENUS and GFP, multitracking in-frame mode was used. VENUS excitation was performed using a 514-nm laser line in conjunction with a 530- to 600-nm band-pass filter. GFP excitation was performed using a 488-nm laser line and collected using a 545-nm secondary dichroic in conjunction with a 505- to 530-nm band-pass filter. The specific sets of filters used for each marker were similar to those described earlier by Gordon et al. (2007) and Su et al. (2009).

Chemical Treatments

NPA (10 mM; Sigma) and estradiol (10 mM; Sigma) stock solutions were prepared in dimethyl sulfoxide and added to SIM at final concentrations of 50 and 10 μM, respectively. Calli were transferred onto fresh medium with estradiol every 2 d. An equal volume of dimethyl sulfoxide was added to the medium in the control experiments.

qRT-PCR Analysis

The primers used in the qRT-PCR analysis are listed in Supplemental Table S4. qRT-PCR was performed for each complementary DNA (cDNA) dilution using the SYBR Green Master mix according to the manufacturer's protocol (Bio-Rad Laboratories). For all samples, cDNAs were normalized using *TUBULIN2* and *ACTIN2*, and the measurements were carried out in three biological replicates. The comparative cycle threshold method, means and SD, was used to calculate and analyze the results (Schmittgen and Livak, 2008)

DNA Microarray Analysis

Total RNAs were isolated from each of the following frozen tissue types: the calli induced on SIM for 0, 4, and 6 d. RNA purification, biotin labeling of complementary RNA, and chip hybridizations were performed by the Affymetrix custom service (CapitalBio). Three biological replicates of each tissue type were analyzed.

An Affymetrix GeneChip Scanner 3000 was used to scan signals from microarray images. GeneChip Operating Software version 1.4 was used to produce MAS4.0 signals and presence-absence calls. Normalization was performed separately for each chip to avoid the introduction of dependencies among biological replications by using dChip 2006 software. Significance Analysis of Microarrays software 2.10 was employed to identify differentially expressed genes between different tissues using fold change of 1.5 or greater and $q < 0.05$ as cutoffs.

Yeast One-Hybrid Analysis

Yeast one-hybrid analysis was performed using a kit (Clontech Laboratories; catalog no. 630491) according to the manufacturer's protocol. Fragments of *AtIPT5* (−24 to −157) and the *AtIPT5* mutant sequence (*AtIPT5m*) were cloned into the *Hin*dIII/*Kpn*I sites of pAbAi, creating pAtIPT5-AbAi and pAtIPT5m-AbAi, respectively. Each of the plasmids, pAtIPT5-AbAi, pAtIPT5m-AbAi, and p53-AbAi, was linearized by digestion with *Bbs*I prior to transformation of the yeast strain Y1HGold. The p53-AbAi construct is a yeast reporter vector that serves as a positive control in the kit (Clontech Laboratories). The full-length cDNA of *ARF3* was isolated and cloned into the pGADT7 activation domain (AD) vector, creating the pAD-ARF3 plasmid. The pAD-ARF3 or empty pGADT7 AD vectors as negative controls were subsequently transformed into the yeast strain containing the pAtIPT5-AbAi or pAtIPT5m-AbAi construct. Activation of the yeast was observed after 3 d on selection plates (synthetic dextrose [SD]/−Leu) containing 100 ng mL^{-1} aureobasidin A (AbA). The primers for ARF cDNA (ARF3-S and ARF3-X) are described in Supplemental Table S4.

SPR Measurements

SPR measurements were performed using a BIAcore-2000 (Pharmacia) at 25°C. The biotin-labeled promoter of *AtIPT5* was immobilized on a streptavidin-coated sensor chip. Dialyzed samples containing ARF3 protein were used as the mobile phase partner, injected at a 20 μL min^{-1} flow rate. The SPR signal in

resonance units was used as a measure of its interaction and kinetics. Data sets were analyzed using CLAMPFIT 8.0 (Axon Instruments).

EMSA

Wild-type and mutated oligonucleotides were commercially synthesized as single-stranded DNA. The wild-type oligonucleotide sequence corresponds to the −130 to −155 region in the *AtIPT5* promoter. The mutated oligonucleotide differed from the wild type in that GAGACA (−143 to −137) had been replaced by TCTCTT. To generate double-stranded oligonucleotides, equal amounts of complementary single-stranded oligonucleotides were mixed, boiled for 2 min, and slowly cooled down to 25°C. For the binding reaction, the LightShift Chemiluminescent EMSA kit (Pierce) was used. For competition experiments, different amounts of nonlabeled wild-type and mutated double-stranded oligonucleotides were used for the binding reaction.

ChIP Assays

The immunoprecipitation of bound chromatin was performed using a ChIP kit (Upstate; catalog no. 17-371) in accordance with the manufacturer's protocol. Calli of the *pARF3*::*ARF3tasiR-GUS* (Marin et al., 2010) transgenic plants, *pMP* (*ARF5*)::*MP-GFP* (Heisler et al., 2005) and *35S*::*6myc-ARF8* plants, and wild-type plants were induced on SIM for 4 d and fixed with 1% (v/v) formaldehyde in growth medium under a vacuum for 10 min at room temperature. Gly was then used to quench unreacted formaldehyde under vacuum for 5 min, and the tissues were ground in liquid nitrogen. Chromatin was then isolated from the tissues, resuspended in SDS lysis buffer with protease inhibitors, and sonicated to achieve an average DNA size of between 0.2 and 1 kb. Next, the chromatin extract was cleared by centrifugation. The ChIP protocol from the kit and antibodies against GUS, GFP, and MYC (Sigma) were then used to obtain purified DNA, which was subsequently analyzed in triplicate by qRT-PCR. Mouse IgG was used as a mock control. For the *35S*::*6myc-ARF8* construct, the *ARF8* coding sequence fragment was amplified and then cloned into the *Bam*HI and *Sac*I sites of the myc-pBA vector. The fold enrichment of the specific chromatin fragment was normalized to the expression levels of the *UBQ10* amplicon and was calculated for each amplicon using the following equation: $2^{(Ct\ AtIPT5\ MOCK\text{-}Ct\ AtIPT5\ ChIP)}/2^{(Ct\ UBQ10\ MOCK\text{-}Ct\ UBQ10\ ChIP)}$. The primers used to amplify *ARF8* cDNA (ARF8-L-myc and ARF8-R-myc), *AtIPT5* promoter DNA (fragment a, +39 to −359; fragment b, −850 to −1,133), *AtIPT5*p-F, *AtIPT5*p-R, *AtIPT5*p-F′, and *AtIPT5*p-R′, and *UBQ10* (UBQ10-5 and UBQ10-3) are listed in Supplemental Table S3.

Sequence data generated from the experiments described in this article can be found in the Arabidopsis Genome Initiative or GenBank/EMBL databases under the following accession numbers: *TUB2* (AT5G62690), *WUS* (AT2G17950), *PIN1* (AT1G73590), *YUC1* (AT4G32540), *YUC2* (AT4G13260), *YUC4* (AT4G32540), *YUC6* (AT5G25620), *ARF3* (AT2G24765), *AtIPT1* (AT1G68460), *AtIPT3* (AT3G63110), *AtIPT4* (AT4G24650), *AtIPT5* (AT5G19040), *AtIPT6* (AT1G25410), *AtIPT7* (AT3G23630), *AtIPT8* (AT3G19160), and *AtIPT9* (AT5G20040).

Supplemental Data

The following materials are available in the online version of this article.

Supplemental Figure S1. Redistribution of auxin and cytokinin responses within the callus on SIM incubation.

Supplemental Figure S2. Localization of PIN1 within the callus during shoot induction.

Supplemental Figure S3. Free indole-3-acetic acid levels were increased in calli after being transferred from CIM onto SIM for 4 d compared with those in the noninduced calli (calli on SIM for 0 d).

Supplemental Figure S4. Relative expression of *ARF3* responds to auxin by qRT-PCR.

Supplemental Figure S5. Shoot regeneration was significantly inhibited in the *ett-1 atipt5-1* double mutant.

Supplemental Table S1. Frequencies of shoot regeneration in the indicated mutants using roots as explants.

Supplemental Table S2. The expression levels of *ARF3* are significantly increased in calli after the transfer onto SIM for 4 and 6 d, which is determined by the Affymetrix Arabidopsis ATH1 Genome Arrays (ArrayExpress accession no. E-MEXP-3120).

Supplemental Table S3. Oligonucleotide sequences and primers used in the yeast one-hybrid, EMSA, SPR, and ChIP assays.

Supplemental Table S4. Primers used in this study.

ACKNOWLEDGMENTS

We thank all who generously provided plant materials or constructs as listed in "Materials and Methods." We also thank Dr. Sharman O'Neill (Department of Plant Biology, College of Biological Sciences, University of California, Davis) for critical reading of the manuscript.

Received August 5, 2012; accepted November 1, 2012; published November 2, 2012.

LITERATURE CITED

Atta R, Laurens L, Boucheron-Dubuisson E, Guivarc'h A, Carnero E, Giraudat-Pautot V, Rech P, Chriqui D (2009) Pluripotency of Arabidopsis xylem pericycle underlies shoot regeneration from root and hypocotyl explants grown *in vitro*. Plant J **57:** 626–644

Bhojwani SS, Razdan MK (1996) Plant Tissue Culture: Theory and Practice, a revised edition. Elsevier Press, New York

Birnbaum KD, Sánchez Alvarado A (2008) Slicing across kingdoms: regeneration in plants and animals. Cell **132:** 697–710

Buechel S, Leibfried A, To JP, Zhao Z, Andersen SU, Kieber JJ, Lohmann JU (2010) Role of A-type *ARABIDOPSIS RESPONSE REGULATORS* in meristem maintenance and regeneration. Eur J Cell Biol **89:** 279–284

Che P, Gingerich DJ, Lall S, Howell SH (2002) Global and hormone-induced gene expression changes during shoot development in *Arabidopsis*. Plant Cell **14:** 2771–2785

Che P, Lall S, Nettleton D, Howell SH (2006) Gene expression programs during shoot, root, and callus development in Arabidopsis tissue culture. Plant Physiol **141:** 620–637

Cheng Y, Dai X, Zhao Y (2006) Auxin biosynthesis by the YUCCA flavin monooxygenases controls the formation of floral organs and vascular tissues in *Arabidopsis*. Genes Dev **20:** 1790–1799

Cheng Y, Dai X, Zhao Y (2007) Auxin synthesized by the YUCCA flavin monooxygenases is essential for embryogenesis and leaf formation in *Arabidopsis*. Plant Cell **19:** 2430–2439

Cheng ZJ, Zhu SS, Gao XQ, Zhang XS (2010) Cytokinin and auxin regulates *WUS* induction and inflorescence regeneration in vitro in *Arabidopsis*. Plant Cell Rep **29:** 927–933

Clough SJ, Bent AF (1998) Floral dip: a simplified method for *Agrobacterium*-mediated transformation of *Arabidopsis thaliana*. Plant J **16:** 735–743

Dello Ioio R, Nakamura K, Moubayidin L, Perilli S, Taniguchi M, Morita MT, Aoyama T, Costantino P, Sabatini S (2008) A genetic framework for the control of cell division and differentiation in the root meristem. Science **322:** 1380–1384

Depuydt S, Hardtke CS (2011) Hormone signalling crosstalk in plant growth regulation. Curr Biol **21:** R365–R373

Dubrovsky JG, Sauer M, Napsucialy-Mendivil S, Ivanchenko MG, Friml J, Shishkova S, Celenza J, Benková E (2008) Auxin acts as a local morphogenetic trigger to specify lateral root founder cells. Proc Natl Acad Sci USA **105:** 8790–8794

Gifford EM, Corson GE (1971) The shoot apex in seed plants. Bot Rev **37:** 143–229

Gordon SP, Chickarmane VS, Ohno C, Meyerowitz EM (2009) Multiple feedback loops through cytokinin signaling control stem cell number within the *Arabidopsis* shoot meristem. Proc Natl Acad Sci USA **106:** 16529–16534

Gordon SP, Heisler MG, Reddy GV, Ohno C, Das P, Meyerowitz EM (2007) Pattern formation during de novo assembly of the *Arabidopsis* shoot meristem. Development **134:** 3539–3548

Guilfoyle TJ, Hagen G (2007) Auxin response factors. Curr Opin Plant Biol **10:** 453–460

Heisler MG, Ohno C, Das P, Sieber P, Reddy GV, Long JA, Meyerowitz EM (2005) Patterns of auxin transport and gene expression during primordium development revealed by live imaging of the *Arabidopsis* inflorescence meristem. Curr Biol **15:** 1899–1911

Jones B, Gunneråas SA, Petersson SV, Tarkowski P, Graham N, May S, Dolezal K, Sandberg G, Ljung K (2010) Cytokinin regulation of auxin synthesis in *Arabidopsis* involves a homeostatic feedback loop regulated via auxin and cytokinin signal transduction. Plant Cell **22:** 2956–2969

Laux T, Mayer KF, Berger J, Jürgens G (1996) The *WUSCHEL* gene is required for shoot and floral meristem integrity in *Arabidopsis*. Development **122:** 87–96

Li W, Liu H, Cheng ZJ, Su YH, Han HN, Zhang Y, Zhang XS (2011) DNA methylation and histone modifications regulate *de novo* shoot regeneration in *Arabidopsis* by modulating *WUSCHEL* expression and auxin signaling. PLoS Genet **7:** e1002243

Lomax TL, Muday GK, Rubery PH (1995) Auxin transport *In* PJ Davies, ed, Plant Hormones and Their Role in Plant Growth and Development. Kluwer Academic Publishers, Boston, pp 509–530

Marin E, Jouannet V, Herz A, Lokerse AS, Weijers D, Vaucheret H, Nussaume L, Crespi MD, Maizel A (2010) miR390, *Arabidopsis TAS3* tasiRNAs, and their *AUXIN RESPONSE FACTOR* targets define an autoregulatory network quantitatively regulating lateral root growth. Plant Cell **22:** 1104–1117

Mayer KF, Schoof H, Haecker A, Lenhard M, Jürgens G, Laux T (1998) Role of *WUSCHEL* in regulating stem cell fate in the *Arabidopsis* shoot meristem. Cell **95:** 805–815

Miyawaki K, Tarkowski P, Matsumoto-Kitano M, Kato T, Sato S, Tarkowska D, Tabata S, Sandberg G, Kakimoto T (2006) Roles of *Arabidopsis* ATP/ADP isopentenyltransferases and tRNA isopentenyltransferases in cytokinin biosynthesis. Proc Natl Acad Sci USA **103:** 16598–16603

Müller B, Sheen J (2008) Cytokinin and auxin interaction in root stem-cell specification during early embryogenesis. Nature **453:** 1094–1097

Murashige T, Skoog F (1962) A revised medium for rapid growth and bioassays with tobacco tissue cultures. Physiol Plant **15:** 473–497

Nordström A, Tarkowski P, Tarkowska D, Norbaek R, Åstot C, Dolezal K, Sandberg G (2004) Auxin regulation of cytokinin biosynthesis in *Arabidopsis thaliana*: a factor of potential importance for auxin-cytokinin-regulated development. Proc Natl Acad Sci USA **101:** 8039–8044

Pekker I, Alvarez JP, Eshed Y (2005) Auxin response factors mediate *Arabidopsis* organ asymmetry via modulation of KANADI activity. Plant Cell **17:** 2899–2910

Pfluger J, Zambryski P (2004) The role of *SEUSS* in auxin response and floral organ patterning. Development **131:** 4697–4707

Reinhardt D, Mandel T, Kuhlemeier C (2000) Auxin regulates the initiation and radial position of plant lateral organs. Plant Cell **12:** 507–518

Ruzicka K, Simásková M, Duclercq J, Petrásek J, Zazímalová E, Simon S, Friml J, Van Montagu MC, Benková E (2009) Cytokinin regulates root meristem activity via modulation of the polar auxin transport. Proc Natl Acad Sci USA **106:** 4284–4289

Schlereth A, Möller B, Liu W, Kientz M, Flipse J, Rademacher EH, Schmid M, Jürgens G, Weijers D (2010) MONOPTEROS controls embryonic root initiation by regulating a mobile transcription factor. Nature **464:** 913–916

Schmittgen TD, Livak KJ (2008) Analyzing real-time PCR data by the comparative $C_{(T)}$ method. Nat Protoc **3:** 1101–1108

Schoof H, Lenhard M, Haecker A, Mayer KF, Jürgens G, Laux T (2000) The stem cell population of *Arabidopsis* shoot meristems in maintained by a regulatory loop between the *CLAVATA* and *WUSCHEL* genes. Cell **100:** 635–644

Sessions A, Nemhauser JL, McColl A, Roe JL, Feldmann KA, Zambryski PC (1997) *ETTIN* patterns the *Arabidopsis* floral meristem and reproductive organs. Development **124:** 4481–4491

Skoog F, Miller CO (1957) Chemical regulation of growth and organ formation in plant tissues cultured *in vitro*. Symp Soc Exp Biol **11:** 118–130

Sohlberg JJ, Myrenås M, Kuusk S, Lagercrantz U, Kowalczyk M, Sandberg G, Sundberg E (2006) *STY1* regulates auxin homeostasis and affects apical-basal patterning of the Arabidopsis gynoecium. Plant J **47:** 112–123

Steeves TA, Sussex IM (1989) Patterns in Plant Development, Ed 2. Cambridge University Press, Cambridge, UK

Su YH, Cheng ZJ, Su YX, Zhang XS (2010) Pattern analysis of stem cell differentiation during *in vitro Arabidopsis* organogenesis. Front Biol **5:** 464–470

Su YH, Liu YB, Zhang XS (2011) Auxin-cytokinin interaction regulates meristem development. Mol Plant **4:** 616–625

Su YH, Zhao XY, Liu YB, Zhang CL, O'Neill SD, Zhang XS (2009) Auxin-induced *WUS* expression is essential for embryonic stem cell renewal during somatic embryogenesis in Arabidopsis. Plant J **59:** 448–460

Tanaka H, Dhonukshe P, Brewer PB, Friml J (2006) Spatiotemporal asymmetric auxin distribution: a means to coordinate plant development. Cell Mol Life Sci **63:** 2738–2754

Ulmasov T, Hagen G, Guilfoyle TJ (1999a) Activation and repression of transcription by auxin-response factors. Proc Natl Acad Sci USA **96:** 5844–5849

Ulmasov T, Hagen G, Guilfoyle TJ (1999b) Dimerization and DNA binding of auxin response factors. Plant J **19:** 309–319

Vanneste S, Friml J (2009) Auxin: a trigger for change in plant development. Cell **136:** 1005–1016

Verdeil JL, Alemanno L, Niemenak N, Tranbarger TJ (2007) Pluripotent versus totipotent plant stem cells: dependence versus autonomy? Trends Plant Sci **12:** 245–252

Vernoux T, Brunoud G, Farcot E, Morin V, Van den Daele H, Legrand J, Oliva M, Das P, Larrieu A, Wells D, et al (2011) The auxin signalling network translates dynamic input into robust patterning at the shoot apex. Mol Syst Biol **7:** 508

Weigel D, Jürgens G (2002) Stem cells that make stems. Nature **415:** 751–754

Weijers D, Schlereth A, Ehrismann JS, Schwank G, Kientz M, Jürgens G (2006) Auxin triggers transient local signaling for cell specification in *Arabidopsis* embryogenesis. Dev Cell **10:** 265–270

Willige BC, Isono E, Richter R, Zourelidou M, Schwechheimer C (2011) Gibberellin regulates PIN-FORMED abundance and is required for auxin transport-dependent growth and development in *Arabidopsis thaliana*. Plant Cell **23:** 2184–2195

Wiśniewska J, Xu J, Seifertová D, Brewer PB, Růžička K, Blilou I, Rouquié D, Benková E, Scheres B, Friml J (2006) Polar PIN localization directs auxin flow in plants. Science **312:** 883

Xu J, Hofhuis H, Heidstra R, Sauer M, Friml J, Scheres B (2006) A molecular framework for plant regeneration. Science **311:** 385–388

Zhao XY, Cheng ZJ, Zhang XS (2006) Overexpression of *TaMADS1*, a *SEPALLATA*-like gene in wheat, causes early flowering and the abnormal development of floral organs in Arabidopsis. Planta **223:** 698–707

Zhao Y (2008) The role of local biosynthesis of auxin and cytokinin in plant development. Curr Opin Plant Biol **11:** 16–22

Zhao Z, Andersen SU, Ljung K, Dolezal K, Miotk A, Schultheiss SJ, Lohmann JU (2010) Hormonal control of the shoot stem-cell niche. Nature **465:** 1089–1092

Zuo J, Niu QW, Frugis G, Chua NH (2002) The *WUSCHEL* gene promotes vegetative-to-embryonic transition in *Arabidopsis*. Plant J **30:** 349–359